# THE MAGNETIC STRUCTURE OF A CORONAL X-RAY BRIGHT POINT

D. S. BROWN[1], C. E. PARNELL[1], E. E. DELUCA[2], L. GOLUB[2] and R. A. MCMULLEN[3]
[1]*Institute of Mathematics, University of St Andrews, St Andrews, KY16 9SS, U.K.*
[2]*Smithsonian Astrophysical Observatory, Cambridge, MA 02188, U.S.A.*
[3]*Department of Physics, Montana State University, Bozeman, MT 59717, U.S.A.*

(Received 17 January 2001; accepted 7 March 2001)

**Abstract.** X-ray bright points are small dynamic loop structures that are observed all over the solar corona. The high spatial and temporal resolution of the TRACE instrument allows bright points to be studied in much greater detail than previously possible. This paper focuses on a specific bright point which occurred for about 20 hours on 13–14 June 1998 and examines its dynamic structure in detail. This example suggests that the mechanisms that cause bright points to form and evolve are more complex than previously thought. In this case, reconnection probably plays a major part during the formation and brightening of the loop structure. However, later on the foot points rotate injecting twist into the bright point which may cause an instability to occur with dynamic results.

## 1. Introduction

X-ray bright points were first observed as 'small concentrated point-like features' by Vaiana *et al.* (1970) during a study of X-ray images of the quiescent solar corona taken during an Aerobee rocket flight in 1969. Krieger, Vaiana, and Speybroeck (1971) first referred to them as 'bright point-like X-ray features observed above bipolar areas in the general coronal field'.

Golub *et al.* (1974) determined the properties of X-ray bright points from a study of *Skylab* X-ray images. They found the lifetime of bright points to be, on average, about 8 hours long and their area to be typically of the order of $2\times10^8$ km$^2$. Bright points starts out as a diffuse cloud which is followed by the growth of a bright core, with an area of the order $10^7$ km$^2$. The maximum area of a bright point is proportional to its lifetime.

It is estimated that as many as 1500 bright points can emerge each day. They are not concentrated in active region belts, but are spread over the surface of the Sun. A second class of longer-lived bright points are thought to exist nearer the equator (Golub, Krieger, and Vaiana, 1976a), with an average lifetime of about 36 hours.

The average temperature of a bright point falls into the range $1.3–1.7\times10^6$ K and the density is typically 2–4 times higher than the coronal average, which is of the order $5\times10^{14}$ m$^{-3}$ (Golub *et al.*, 1974). 5–10% of bright points also show rapid brightening which is consistent with small flares. *Yohkoh* observations suggest that

*Solar Physics* **201:** 305–321, 2001.


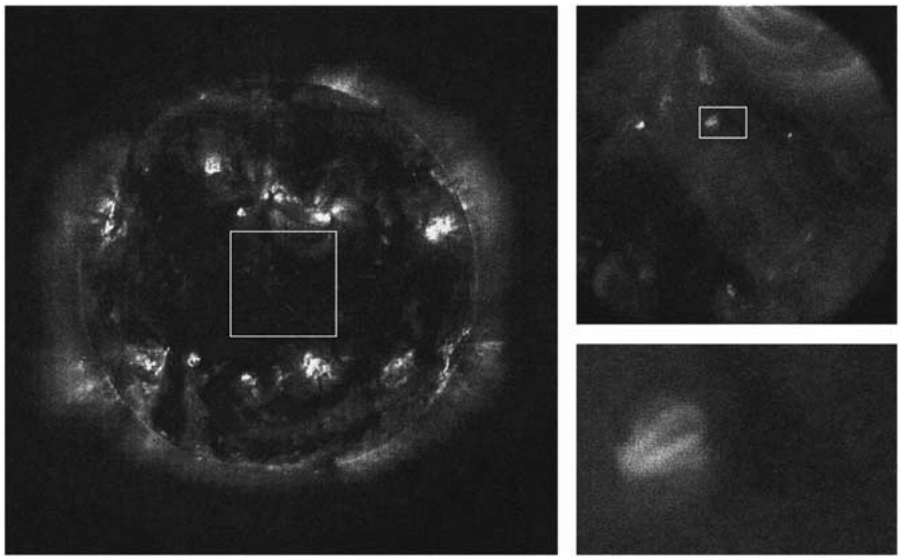

*Figure 1.* EIT image (*left*) of the Sun at 07:14 UT on 14 June 1998 showing the region which TRACE was observing (*right top*) which in turn shows the clipping region of the bright point (*right bottom*).

bright points fluctuate in intensity by 30–200% over time-scales of a few minutes to hours (Priest, Parnell, and Martin, 1994).

*Skylab* observations suggested that bright points have a size of about 20 Mm, but in the 1990s NIXT (which had a higher resolution and lower scatter than Skylab) observed complex loop structure in bright points with a size of the order 9 Mm (Parnell, Priest, and Golub, 1994; Parnell, 1994).

Bright points are typically associated with small bi-polar magnetic features in the photosphere which have a typical total flux of $10^{19}-10^{20}$ Mx (Golub, Krieger, and Vaiana, 1976b). It is thought that, at most, one third of bright points lie over ephemeral regions, which are newly emerging regions of magnetic flux, whereas the remaining two thirds lie above *canceling magnetic features*, which consist of opposing polarity fragments that approach one another and disappear (Harvey, 1985; Harvey *et al.*, 1993; Webb *et al.*, 1993). This led Priest, Parnell, and Martin (1994) to propose a converging flux model where the approaching flux regions of a bi-pole cause a null point to rise out of the photosphere. The bright point is then powered by energy from reconnection at this null point.

More recently, bright points have been observed by the EIT instrument on SOHO and then, in 1998, TRACE enabled both high temporal and spatial observations of bright points to be made. Traditionally, the name X-ray bright point has been used, even though both EIT and TRACE image the corona in extreme ultraviolet light.

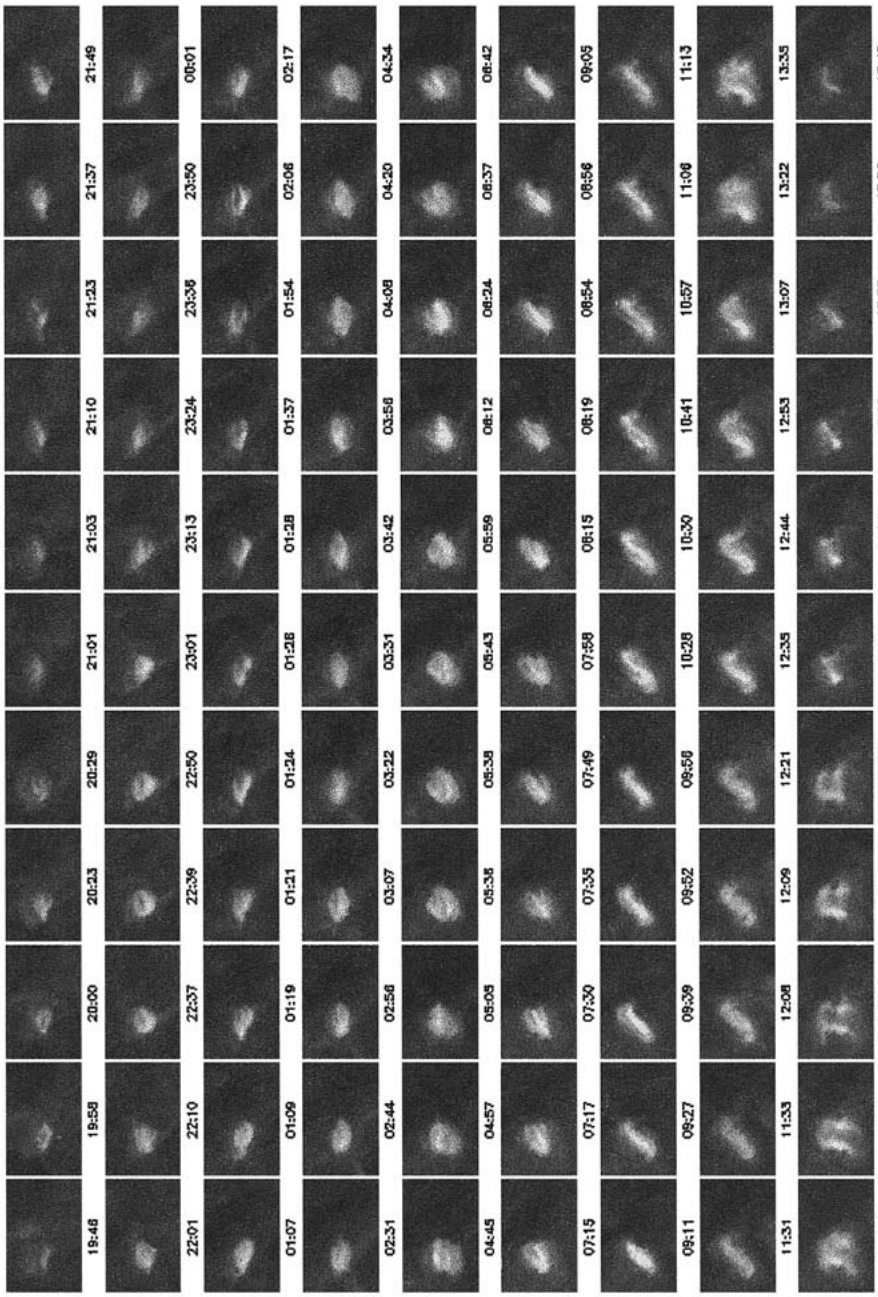


*Figure 2.* Evolution of a coronal bright point observed in Fe XII by TRACE on 13 and 14 June 1998. Each frame is $75 \times 50$ arc sec$^2$. All time data here, as well as in other figures, and everywhere in the text, are in UT.

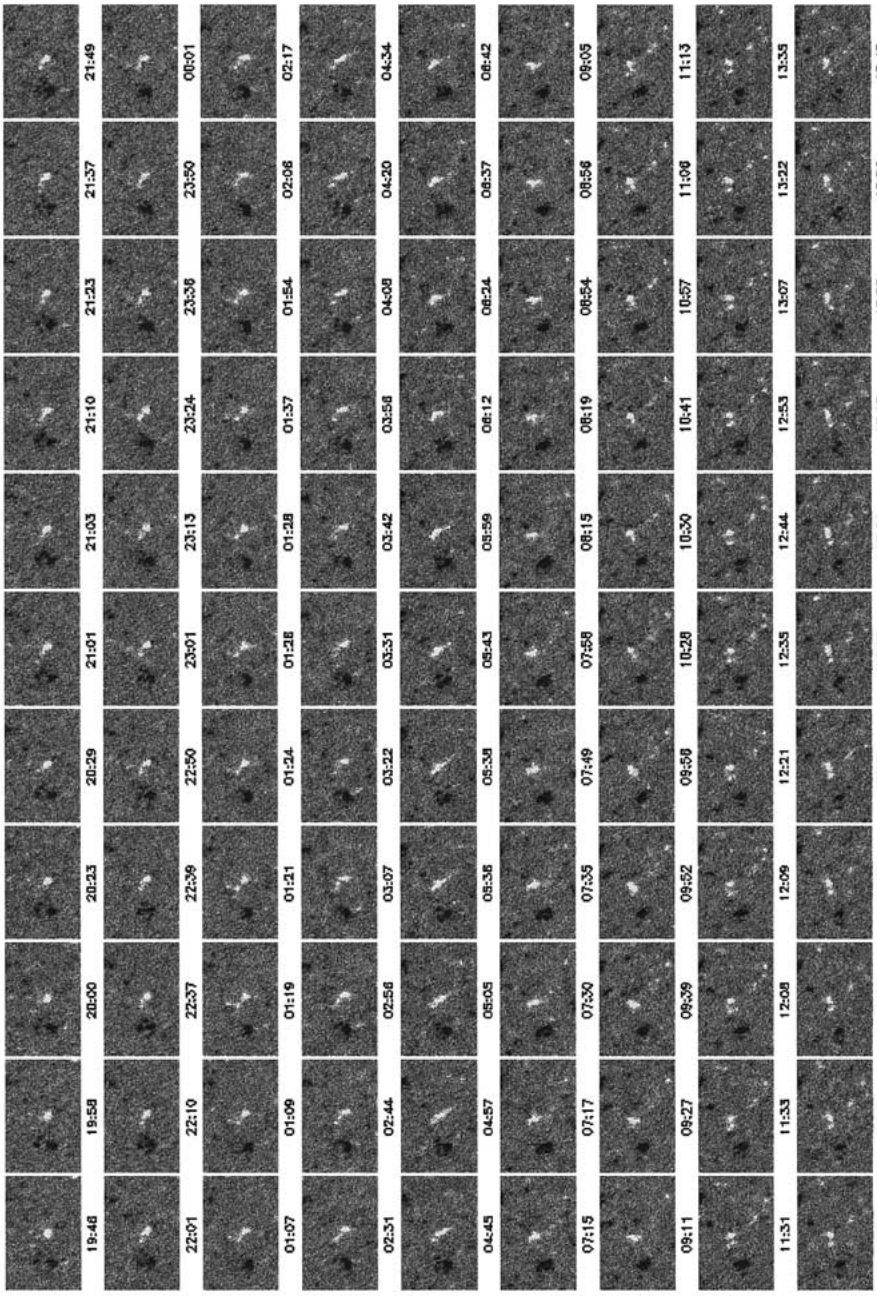


*Figure 3.* Evolution of the magnetic fragments responsible for the coronal bright point in Figure 2, in magnetograms observed by SOHO/MDI. Each frame is $75 \times 50$ arc sec$^2$.

## 2. Bright Point Observations

From 13–17 June 1998, TRACE and SOHO/MDI simultaneously observed the same quiet region of the Sun. From these observations the fascinating and complex structure of bright points can be seen in great detail. One particular bright point, which lasted for about a day, exhibited dynamic structural behavior which became increasingly complex and led to its sudden eruptive demise.

This bright point has been extracted from the quiet-Sun TRACE observation sequence and is completely contained within the MDI high-resolution field of view, passing approximately 60 arc sec above disk center. The region extracted is 75 arc sec by 50 arc sec and runs over a period of about 22 hours. Figure 1 shows an EIT image which indicates the region of the Sun which TRACE was observing and a TRACE image from which the bright point region was clipped. Due to rotation of the Sun, the bright point actually moves across the image from left to right, so the clipped region is moved accordingly.

Image cubes from the Fe IX and Fe XII (Figure 2) lines of TRACE and from MDI high-resolution magnetograms (Figure 3) have been extracted and de-rotated to eliminate lateral movement, allowing a morphological study to be carried out. The TRACE data has also been de-spiked (i.e., has had cosmic rays removed) and the dark current across the CCD has been subtracted. The Fe IX observations were taken at a spatial resolution of 0.5 arc sec per pixel, while the Fe XII observations were taken at 1 arc sec per pixel. The exposure times of the Fe XII observations are not constant so data has been normalized to compensate. The high-resolution magnetograms have a resolution of approximately 0.605 arc sec per pixel.

In general, the cadence is under 2 min between frames of the same filter band, though there are larger gaps where data has been corrupted or when TRACE was performing synoptic duties.

## 3. Behavior of the Bright Point

The bright point (Figure 2) appears at around 20:00 on 13 June and continues to grow and brighten over the next 12 hours. It then begins to twist forming a sigmoid shape which lasts for the next 4 hours. This twist phase is followed by another 2.5-hour period in which the bright point is seen to have dramatically changed its structure to that of a $\pi$ shape, before it disappears.

The bright point can be defined as being made up of pixels which, statistically speaking, are higher than background intensity. The intensity range covered by the background intensity is well fitted by a Gaussian curve, with the bright point producing a skewed tail at the high end of the distribution (Figure 4).

Using this definition, several characteristics of the bright point are calculated. Figure 5 shows how the area of the bright point evolves over time. The bright point

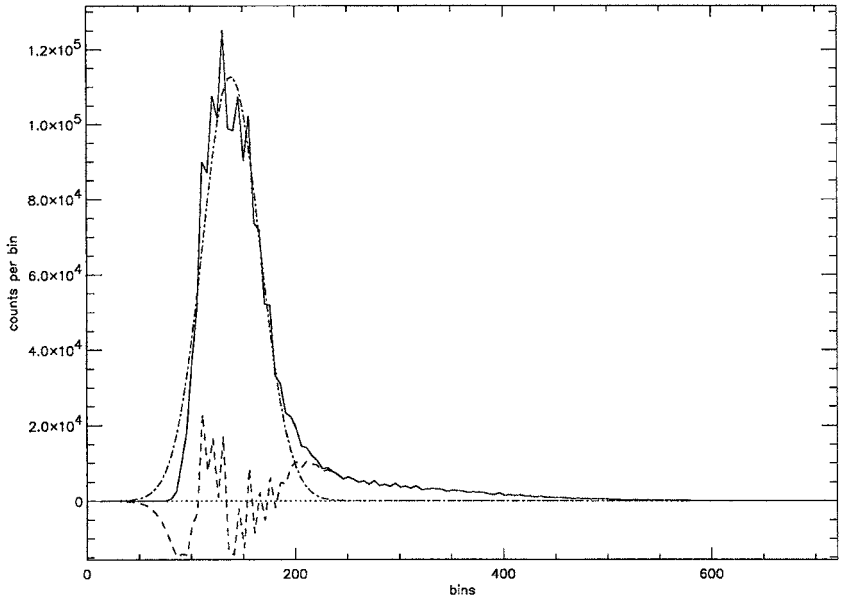


*Figure 4.* Plot showing the spread in pixel intensity values of the bright point observations in the Fe XII line (*solid*). A Gaussian curve (*dot-dash*), which represents the background intensity, is fitted to this and subtracted, the resulting curve (*dashed*) shows the 'tail' of the intensity curve, which is defined as being due to bright point pixels alone.

slowly grows over the course of about 20 hours to a peak associated with the $\pi$ phase, after which it dramatically shrinks and fades.

Golub *et al.* (1974) suggest that the maximum area is proportional to the lifetime of the bright point according to the relation

$$A_{\max} = 2.5 \times 10^7 \tau, \tag{1}$$

where $\tau$ is measured in hours and $A_{\max}$ in km$^2$.

The lifetime of the bright point is about 22 hours and the maximum size it reaches is about 950 arc sec$^2$, which is approximately $5 \times 10^8$ km$^2$. This is in reasonable agreement with Equation (1) which predicts a maximum area of $5.5 \times 10^8$ km$^2$.

Key to the behavior of the bright point is the behavior of the magnetic fragments in the photosphere, where the bright loops have their footpoints. There are two large fragments, one positive (white patch in Figure 3) and one negative (black patch in Figure 3), that remain throughout the life of the bright point. The positive fragment migrates north as the bright point progresses.

There are some smaller negative fragments near the main one, forming a 'paw print' shape (from 19:26 onwards). As the bright point evolves, these fragments approach the main one, forming a larger negative fragment (at about 23:30). These fragments (or new ones) later split from the main fragment (at about 03:20) to reform the 'paw print' shape. The fragments coalesce once more (at about 07:00)

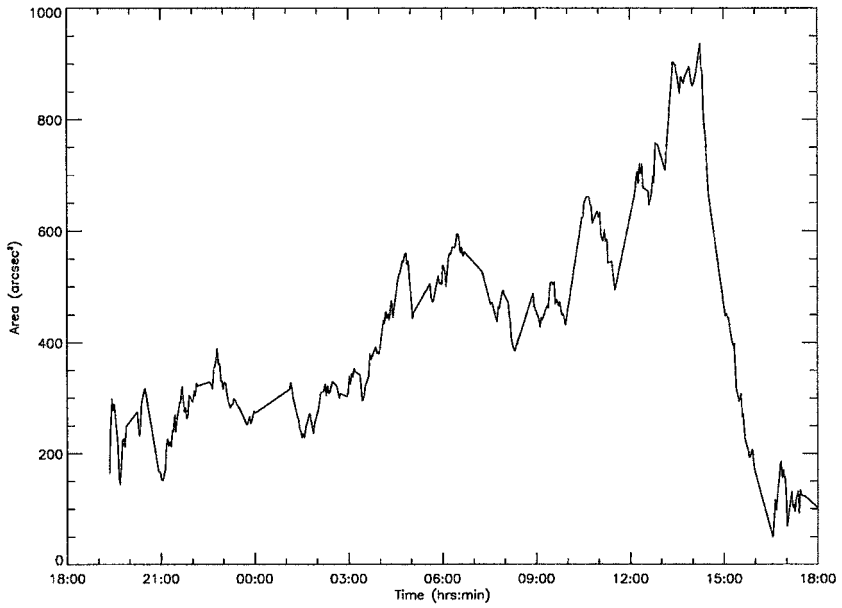


*Figure 5.* Plot showing the change in area of the bright point over the course of its lifetime.

to form a single fragment. A second smaller fragment starts to emerge (at about 11:00) and remains for the rest of the bright point's life.

At the beginning of the life of the bright point there is only the main positive fragment. This fragment splits into two smaller fragments (at about 23:00), one of which splits again (at about 02:30). These fragments then coalesce (at about 05:00). This single fragment is joined by several smaller fragments (at about 10:00) which appear below the main fragment and migrate north. At this point the main positive fragment separates into two smaller fragments. This is summarized in Table I.

It is also important to look at the flux passing through the photosphere due to these key fragments. Figure 6 shows the total positive flux and the total negative flux from the significant fragments. Note that there is no evidence of flux cancellation (except when the bright point fades) and the MDI observations (Figure 3) do not show the two main fragments approaching one another. This suggests that the bright point is not above a *canceling magnetic feature* (Section 1).

Figure 6 indicates four key phases during the life of the bright point. First, the positive flux is stronger than the negative flux, but at about 00:00 the two flux strengths approach the same level. They remain approximately equal until about 07:30 when the negative flux increases and dominates over the decreasing positive flux. Finally, at about 15:00 the negative flux decreases to the level of the positive flux and they both tail off equally as the bright point dies.

These changes in behavior of the magnetic fragments are prime candidates for changes in the behavior of the bright point. The first major change occurs between 23:00 and 00:00 and is reflected in the behavior of the positive and negative frag-

TABLE I

Summary of the behavior of the bright point and the magnetic fragments in the photosphere.

| Time (UT) | Bright point behavior | Magnetic fragment behavior |
|---|---|---|
| 19:30 | The bright point emerges becoming larger and brighter. | The single positive fragment dominates the negative fragments which form a 'paw print.' |
| 23:00 | The bright point deforms from a blurred blob into distinct loops. | The negative fragments coalesce and become as strong as the positive fragment which splits into two separate fragments. |
| 03:00 | The distinct loops begin to merge into a bright indistinguishable blur. | The negative fragment splits into a 'paw print' once more. |
| 05:30 | | The two positive fragments coalesce into a single fragment. |
| 06:40 | The blur begins to resolve itself into distinguishable loops once more, which begin to twist. | The negative fragments coalesce and begin to dominate the positive fragments. |
| 10:00 | The bright point becomes even more twisted into its sigmoid phase | Small positive fragments start to approach the bright point from below. |
| 11:00 | | A new negative fragment begins to emerge near the existing negative fragment. |
| 13:00 | The twist becomes too much and the structure breaks into a $\pi$-shape. | The positive fragments have become closer to the bright point and the number of significant fragments has dramatically increased. |
| 15:00 | A large portion of the bright point has dispersed leaving some smaller loops which quickly fade. | Many of the fragments disappear as the bright point is dispersed leaving smaller more balanced fragments |

ments and their relative strengths. The only noticeable change in the behavior of the bright point at this time is that the brighter 'blobs' in Figure 2 begin to resolve themselves into more definite loop structures.

The next significant change occurs at about 07:00, when the negative fragments coalesce and the total negative flux becomes greater than the positive negative flux. It is about this point that the bright point loops begin to twist into the sigmoid shape.

The splitting of the main fragments and the introduction of the new positive fragments that occurs from 10:00 onwards could contribute to the change in shape from the sigmoid to the $\pi$-structure, but this is likely to be dominated by the stress of the twisting loops.

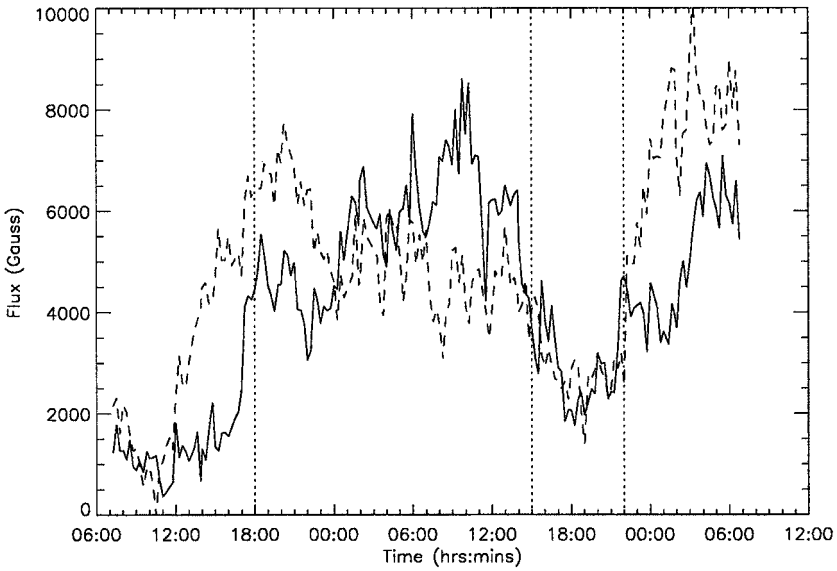


*Figure 6.* Plot showing the variation of flux passing through the magnetogram from 7 hours before the bright point emerges to 15 hours after it dies. The *dashed line* shows the total flux from significant positive fragments, the *solid line* shows the total flux from significant negative fragments. The lifespan of the bright point is indicated by the *dotted lines* at 18:00 and 15:00. There is a third line at 22:00 which indicates the appearance of another bright point in the region.

## 4. Birth of the Bright Point

Figure 6 also shows the buildup of significant fragments of positive and negative flux several hours before the bright point is initially visible. This could indicate that the two main fragments are emerging and that the bright point lies above an ephemeral region. However, a close study of the magnetograms, before the bright point emerges, suggests a different explanation.

Both the main positive and negative fragments exist at least seven hours before the bright point emerges. At this time they are not strong, but they lie at the intersections of supergranule cells near to regions of strong down-flow (one for the positive fragments and one for the negative fragments). These, and other small fragments that exist or emerge nearby, are caught in the down-flow and coalesce to form larger fragments with higher strength (Figure 7). These two down-flow regions are probably on opposite sides of the same supergranule cell, evidence for this is that the two regions are approximately 20 arc sec apart (which is a reasonable size for a supergranule cell) and the paths of smaller fragments give a partial outline for a supergranule cell. Also, the two poles do not approach one another during the life of the bright point, which suggests that they are on opposite side of a supergranule cell rather than on the same vertex.

When the expanding fragments reach a certain strength (the total flux of the fragments becomes about $8-10 \times 10^3$ G-pixel), the bright point begins to form (at

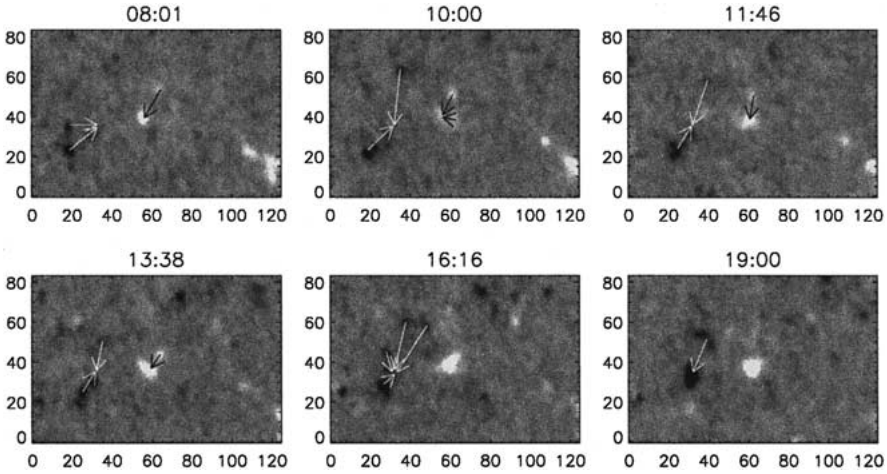


*Figure 7.* Magnetograms showing the bright point region before its emergence. The main positive and negative fragments grow as other fragments merge with them.

around 18:00 on the 13th). When the total flux falls below this threshold the bright point dies (around 15:00 on the 14th). A new bright point emerges close by several hours later, involving some of the positive fragment from the previous bright point.

## 5. The Early Stages of the Bright Point

During the first half of the lifetime of the bright point (20:00–05:30), the magnetic fragments undergo coalescence and fragmentation, the negative fragment in particular splits into several smaller sources which later coalesce.

As the small fragments initially approach to form the sources for the main bipole pair, magnetic separators are created (Longcope, 1998; Brown and Priest, 1999b). Separators are magnetic field lines that connect two null points and border four regions of connectivity. In an MHD scenario, it is believed that a separator can develop into a current ribbon where reconnection can occur (Longcope, 1996).

It is thought (Longcope, 1998) that reconnection at separators/current ribbons releases energy which heats the plasma and causes loop structures to brighten. This is likely to be the main cause of the brightening studied in this paper. A topological investigation of the bright point shows that when the magnetic sources in the photosphere fragment then separators occur (see Brown and Priest, 1999a, for a discussion of magnetic topology). Figure 8 shows some examples of this selected from the first half of the bright points life. In each case there is a separator (indicated by a black dashed line) close to the active area of the bright point.

The separators are caused by the magnetic sources of the dipole fragmenting into smaller flux patches (Figure 9). The motion of these small fragments causes magnetic flux to reconnect through the current ribbon so that the footpoints of

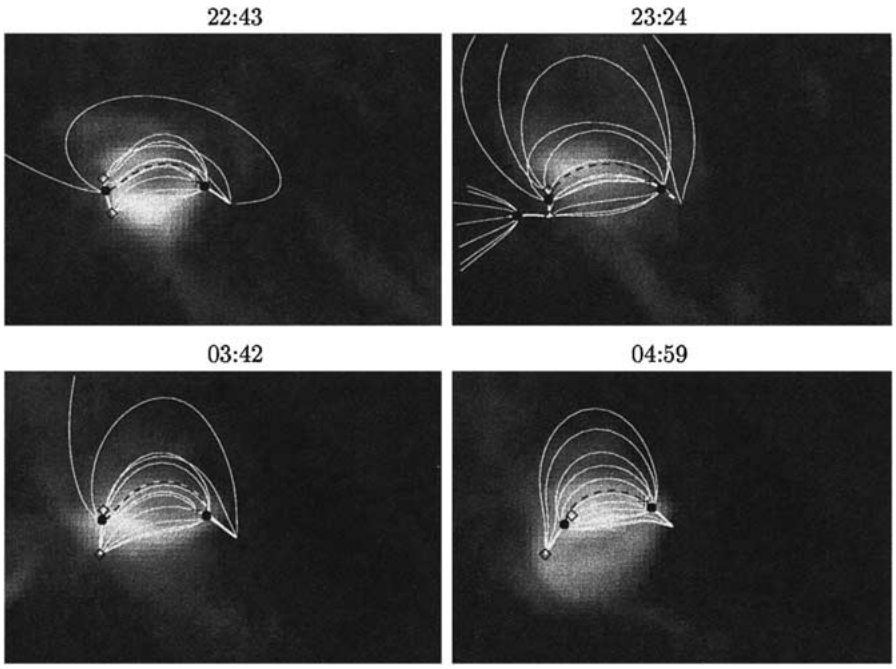


*Figure 8.* A selection of potential topologies of the bright point viewed from above. The *white lines* indicate the separatrix surfaces and the *black dashed lines* show the position of the separators. Sources are indicated by *pluses* (positive) and *diamonds* (negative) and null points by *dots*.

field lines changes from one fragment to another. This allows the loop structure to remain bright throughout the first half of the life of the bright point.

Potential modeling has been used to construct these topologies. The bright point is unlikely to be potential but it is believed that the topology, and therefore the separator, is robust enough to exist in higher-order models (Brown and Priest, 2000).

## 6. The Sigmoid-Phase

From about 5:30 to 13:00 the bright point twists and forms a sigmoid. The cause of this twist is rooted in the photosphere and the high resolution and cadence of the SOHO/MDI magnetograms shows that the main positive and negative fragments undergo a clockwise rotation as the bright point loops twist (Figure 10).

From the beginning of the fragment's rotation at about 05:30 to the end of the rotation and its subsequent split into two smaller fragments at about 13:00, the orientation of the positive magnetic feature undergoes a turn of approximately $3\pi/4$ radians.

Rotation of the negative fragment is less obvious as it undergoes a more dramatic change of shape as small sources coalesce with it which makes determining

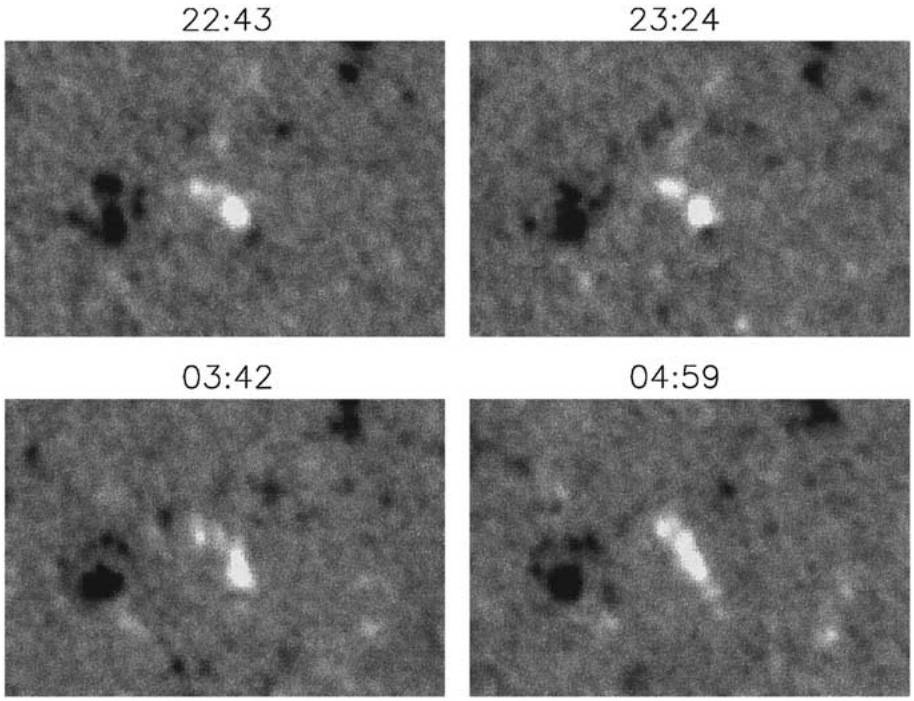


*Figure 9.* High-resolution SOHO/MDI magnetograms corresponding to the extrapolated topologies in Figure 8. The two poles are resolved to be clusters of smaller fragments, the motion of which could cause reconnection in the bright point.

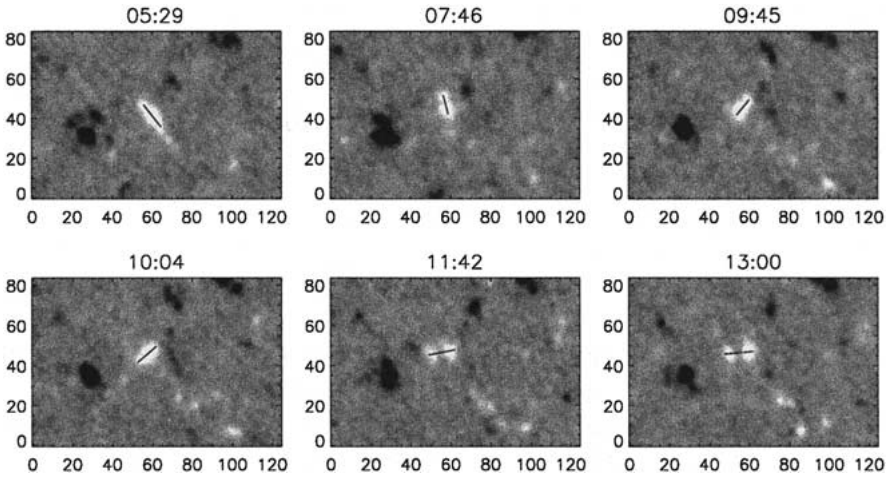


*Figure 10.* The positive (*white*) fragment rotates approximately $3\pi/4$ radians clockwise over the space of 7–8 hours.

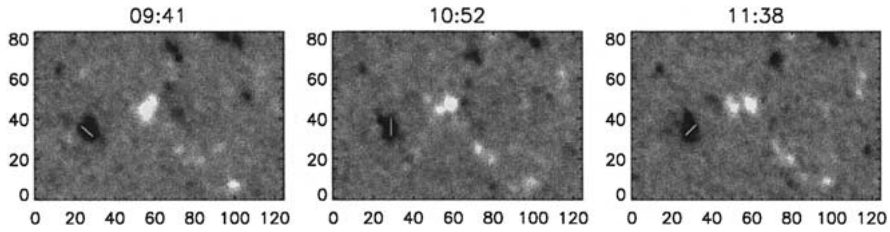


*Figure 11.* The negative (*black*) fragment rotates approximately $\pi/2$ radians clockwise over the space of about 2 hours.

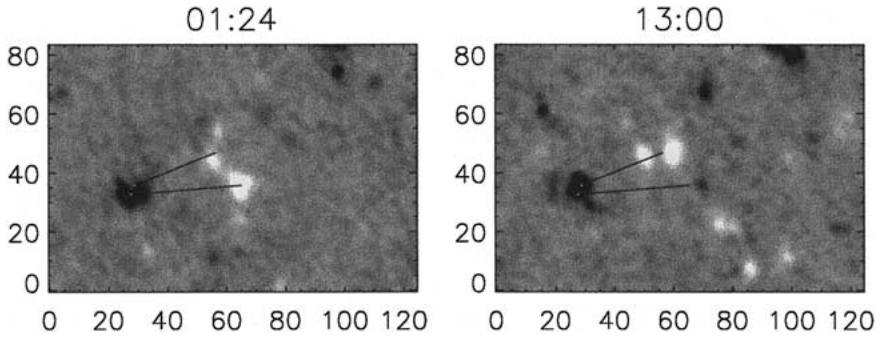


*Figure 12.* The positive (*white*) fragment drifts north during the lifetime of the bright point. The angle it moves relative to the negative (*black*) fragment is approximately $\pi/10$ radians.

the rotation difficult. However, it does appear to undergo a rotation of about $\pi/2$ radians clockwise over the space of two hours from 09:41 to 11:38 (Figure 11). As the two fragments rotate in the same direction (clockwise) then the twist they apply is cumulative. So the total twist provided by the fragments rotating is about $5\pi/4$ radians.

As well as the undergoing rotation, the positive fragment also drifts north about 14 arc sec. In relation to the negative fragment, the positive fragment moves through an angle of approximately $\pi/10$ radians (see Figure 12). This drift contributes twice this angle to the twist (as both foot-points have undergone an effective turn of $\pi/10$ radians), so the total twist from the rotating foot-points and the shear from the northern drift is just under $3\pi/2$ radians (the twist and shear is cumulative in this case, if the fragment drifted south, or the fragments rotated anti-clockwise then the shear would remove twist).

A crude estimate of the twist injected into the loop structure can be made by calculating the angle at which the loop structure (seen in the TRACE Fe XII observations) enters each footpoint relative to the chord between the two foot-points at the beginning and end of the sigmoid phase. Figure 13 shows two observations at the beginning of the sigmoid phase and two from the end. On each image a possible loop path has been sketched and the angle between the loop and the chord between the foot-points is measured. The loop end over the positive fragment sweeps through an angle of between $0.65-0.75\pi$ clockwise and the loop end over

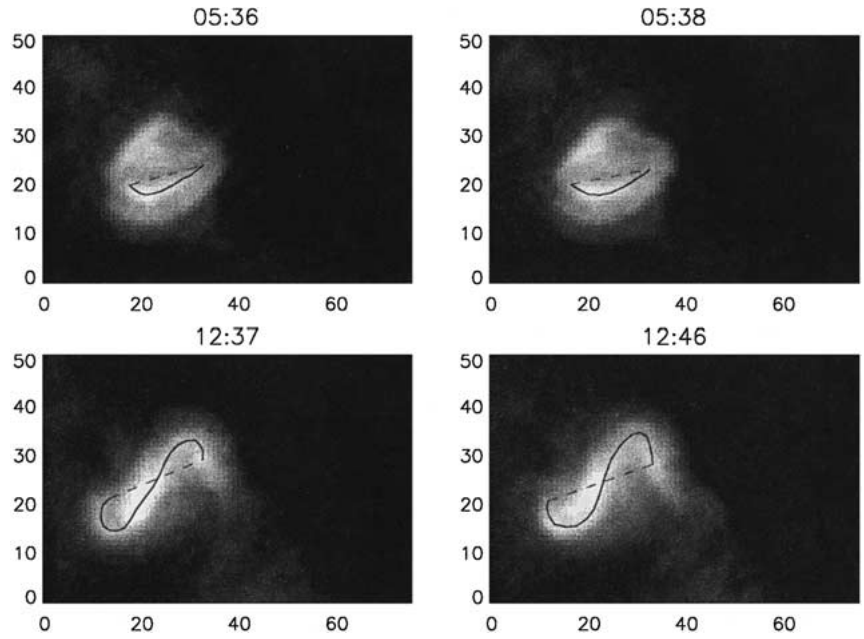


*Figure 13.* Possible loop paths overlaid onto the Fe XII data from TRACE at the beginning and end of the sigmoid phase.

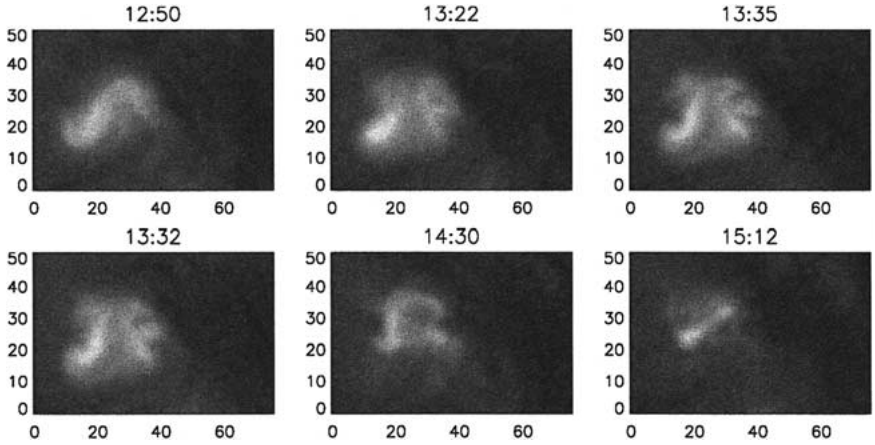


*Figure 14.* The $\pi$-shaped structure quickly develops from the sigmoid and fades to a small loop structure over the space of about 2 hours.

the negative fragment sweeps though an angle of between $0.35-0.45\pi$ clockwise. This gives a total twist of approximately $1-1.2\pi$ to the bright point.

Despite the fact that this method is crude and subjective, this gives a reasonable correspondence with the twist of the foot-points. In each case the twist given by the Fe XII observations is slightly less than the twist seen in the magnetic fragments which suggests that there is some reconnection occurring.

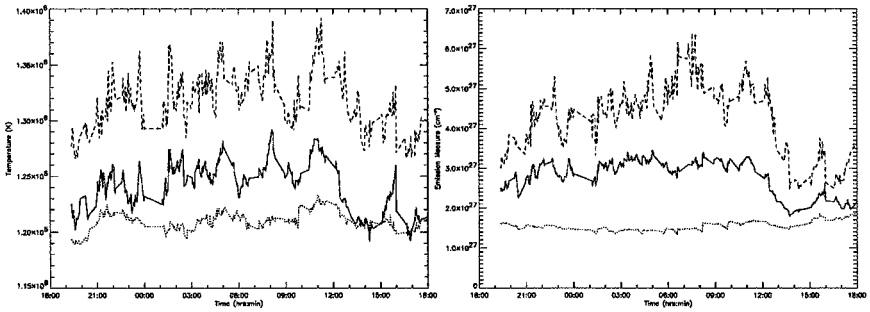

*Figure 15.* Plots of (*left*) the average temperature and (*right*) emission measure of the bright point. The *solid line* shows the average temperature/EM of the bright point, the *dashed line* shows the peak temperature/EM of the bright point, and the *dotted line* shows the average temperature/EM of the background.

Theoretical experiments suggest that for a loop to become unstable it must undergo a twist of $2-2.5\pi$ (Arber, Longbottom, and Van Der Linden, 1999). However, such experiments use very simple magnetic fields in a cylindrical geometry, and it is not known how a complex magnetic field (such as in the corona) will affect this.

## 7. The $\pi$-Phase

When the sigmoid structure breaks, it is rapidly replaced by a $\pi$-shaped structure which fades over the space of about 2 hours to a small untwisted loop structure which itself fades, signaling the death of the bright point (Figure 14). The flux passing through the bipole rapidly reduces (Figure 6) and the remainder of the two fragments move apart (the positive fragment later forms another bright point with a different negative fragment).

One would intuitively say that the sigmoid erupts into the $\pi$-phase and there is some evidence to support this. By taking ratios of the Fe XII and Fe IX observation bands and applying a temperature scaling the temperature diagnostic of the bright point can be studied over the course of its life. Passing these temperature through an appropriate response function will then give information about the emission measure, which is proportional to the square of the number density (see, for example, Klimchuk and Gary, 1995).

Figure 15 shows how the average temperature and emission measure of the bright point (as identified by Figure 4) vary over its lifetime. At approximately 12:30 there is a sudden drop in both the temperature and emission measure of the bright point which coincides with the changing of the sigmoid into the $\pi$-structure. Temperature diagnostics with the Fe IX and Fe XII bands pick out plasma within the range of 0.9–1.6 million degrees. This sudden drop in temperature and emission measure could be caused by the hotter plasma being ejected from the bright point

(and perhaps being rapidly heated above the detectable range of TRACE). This would be consistent with the sigmoid becoming unstable and reconnecting which would cause plasma to be heated and ejected.

## 8. Conclusions and Discussion

This paper has studied in detail the complete life of a single coronal bright point. This example displays four main stages of evolution, the pre-brightening stage, the initial brightening, the sigmoid-phase and the $\pi$-phase.

The pre-brightening stage shows that this particular bright point is formed between two down-flow regions into which small positive or negative fragments, some newly emerged, enter and coalesce to form the larger positive and negative fragments of a bipole. Brightening occurs after the bipole undergoes a dramatic increase in flux. It is likely that the two poles form on either side of a supergranule cell.

During the early stages of the bright point the sources of the bipole fragment and coalesce. Fragmentation causes the creation of separators at which current sheets may form and reconnection occurs. This is responsible for the initial heating of the plasma in the bright point.

About half way though the life of the bright point, the loop structure starts to twist into a sigmoid. This is in response to rotation and translation of the magnetic fragments in the photosphere. These factors inject a combined twist of approximately $3\pi/2$ radians (although some of this may be dispersed through reconnection). At this critical twist the sigmoid may become unstable and erupt into the $\pi$-phase.

There is some evidence that material is ejected from the bright point at the onset of the $\pi$-phase; however, this involves taking the ratio between two different EUV bands on TRACE and the assumptions that go into that (such as assuming the plasma is isothermal and isochronic when generating the band response curves).

The $\pi$-shape fades to a smaller loop structure which quickly fades, signaling the end of the bright point. The dying bright point is associated with a large drop in the amount of flux passing through the bipole fragments.

This paper has just focused on one bright point, it is unclear which behavior is specific to this bright point or whether other bright points display similar behavior. It does suggest that bright points are more dynamic and complex than previously thought and exhibit different behavior at different stages of their life time. Further work with more bright points would be required to establish this.

## 9. Included on the CD-ROM

With this paper are observation stills and movies located on the accompanying CD-ROM. These are: a copy of Figure 2, the TRACE Fe XII observations, displayed with a red-scale color scheme; the equivalent TRACE Fe IX observations; a movie showing the evolution of the bright point in the TRACE Fe XII, Fe IX, and L$\alpha$ bands and the SOHO/MDI magnetograms; an enlarged movie of the SOHO/MDI magnetograms with observations starting several hours before and finishing several hours after the life of the bright point.

## Acknowledgements

DSB would like to thank the Particle Physics and Astronomy Research Council and CEP would like to thank the Royal Astronomical Society for financial support. DSB and CEP would like to thank the Smithsonian Astrophysical Observatory for travel support.

## References

Arber, T. D., Longbottom, A. W., and Van Der Linden, R. A. M.: 1999, *Astrophys. J.* **517**, 990.
Brown, D. S. and Priest, E. R.: 1999a, *Proc. Royal Soc.* **455**, 3931.
Brown, D. S. and Priest, E. R.: 1999b, *Solar Phys.* **190**, 25.
Brown, D. S. and Priest, E. R.: 2000, *Solar Phys.* **194**, 197.
Golub, L., Krieger, A. S., and Vaiana, G. S.: 1976a, *Solar Phys.* **49**, 79.
Golub, L., Krieger, A. S., and Vaiana, G. S.: 1976b, *Solar Phys.* **50**, 311.
Golub, L., Krieger, A. S., Silk, J., Timothy, A., and Vaiana G. S.: 1974, *Astrophys. J.* **198**, L93.
Harvey, K. L.: 1985, *Aust. J. Phys.* **38**, 875.
Harvey, K. L., Nitta, N., Strong, K. T., and Tsuneta, S.: 1993, in *X-ray solar physics from Yohkoh. Frontiers Science Series, Proceedings of the International Symposium on the Yohkoh Scientific Results*, 21.
Klimchuck, J. A. and Gary, D. E.: 1995, *Astrophys. J.* **448**, 925.
Krieger, A. S., Vaiana, G. S., and Speybroeck, L. P.: 1971, 'Solar Magnetic Fields', *IAU Symp.* **43**, 397.
Longcope, D. W.: 1996, *Solar Phys.* **169**, 91.
Longcope, D. W.: 1998, *Astrophys. J.* **507**, 433.
Parnell, C. E.: 1994, *Proc. of the Third SOHO Workshop - Solar Dynamic Phenomena and Solar Wind Consequences*, p. 149.
Parnell, C. E., Priest, E. R., and Golub, L.: 1994, *Solar Phys.* **151**, 57.
Priest, E. R., Parnell, C. E., and Martin, S. F.: 1994, *Astrophys. J.* **427**, 459.
Vaiana, G. S., Krieger, A. S., Speybroeck, L. P., and Zehnpfennig, T.: 1970, *Bull. Am. Phys. Soc.* **15**, 611.
Webb, D. F., Martin, S. F., Moses, D., and Harvey, J. W.: 1993, *Solar Phys.* **144**, 15.